Number of words: 4600

Number of figures:7

Number of tables:1

Finite Element Modelling of Radial Shock Wave Therapy for Chronic Plantar Fasciitis

Zaied K. Alkhamaali[1,2]

Andrew D. Crocombe[1]

Matthew C. Solan[3]

Srdjan Cirovic[1,2]

[1]The Centre for Biomedical Engineering

[2]Department of Mechanical Engineering Sciences

University of Surrey, Guildford, Surrey, GU2 7XH, UK

[3]Department of Orthopaedic Surgery, Royal Surrey County Hospital, Guildford, Surrey, GU2 7XX, UK

Corresponding Author:

Srdjan Cirovic

The Centre for Biomedical Engineering

University of Surrey, Guildford, GU1 7XH, UK

Tel.:+44 (0)1483 686734

s.cirovic@surrey.ac.uk

Finite Element Modelling of Radial Shock Wave Therapy for Chronic Plantar Fasciitis

Therapeutic use of high-amplitude pressure waves, or shock wave therapy, is emerging as a popular method for treating musculoskeletal disorders. However, the mechanism(s) through which this technique promotes healing are unclear. Finite element models of a shock wave source and the foot were constructed to gain a better understanding of the mechanical stimuli that shock wave therapy produces in the context of plantar fasciitis treatment. The model of the shock wave source was based on the geometry of an actual radial shock wave device, in which pressure waves are generated through the collision of two metallic objects: a projectile and an applicator. The foot model was based on the geometry reconstructed from magnetic resonance images of a volunteer and it comprised bones, cartilage, soft tissue, plantar fascia, and Achilles tendon. Dynamic simulations were conducted of a single and of two successive shock wave pulses administered to the foot. The collision between the projectile and the applicator resulted in a stress wave in the applicator. This wave was transmitted into the soft tissue in the form of compression-rarefaction pressure waves with an amplitude of the order of several MPa. The negative pressure at the plantar fascia reached values of over 1.5 MPa, which could be sufficient to generate cavitation in the tissue. The results also show that multiple shock wave pulses may have a cumulative effect in terms of strain energy accumulation in the foot.

Key Words: shock wave therapy, plantar fasciitis, finite element modelling

1 Introduction

Plantar fasciitis is a painful condition in the tough band of connective tissue along the sole of the foot, affecting ten percent of the general population during the course of a lifetime (Crawford et al., 2002, Rome and Saxelby, 2005). Shock wave therapy, a therapeutic use of high-amplitude transient pressure waves, is an increasingly popular treatment method for plantar fasciitis, especially in the cases where conservative treatments such as stretching, taping or orthoses fail to be effective (League, 2008, Rome and Saxelby, 2005, Rompe et al., 2007). Shock wave therapy (SWT) was originally developed as a non-invasive technique for breaking kidney stones, but the scope of its application quickly widened. Currently, SWT is used to treat a number of musculoskeletal disorders including: plantar fasciitis, Achilles tendinitis, patellar tendonitis, and others (Wang, 2012). There are two forms of SWT: focused and radial. In focused shock wave therapy (fSWT) the whole energy of a shock wave is concentrated in a small treatment zone within the body. In radial shock wave therapy (rSWT) the pressure is generated through the collision of two metal objects: a compressed air-driven 'projectile' and an 'applicator' which is pressed against the skin with a force of over 30 N and coupled with an ultrasound gel. From the surface of the body, pressure waves spread in all directions, eventually reaching the affected zone. In-vitro experiments show that this method generates maximal positive and negative pressure (P_+ and P_-, respectively) near the applicator tip of up to 10 MPa, and an energy flux density (EFD) in the low-to-medium range (EFD< 0.28 mJ mm^{-2}) (McClure and Dorfmuller, 2003). However, both the pressure amplitude and the energy drop rapidly with distance and may be substantially lower in the treatment zone. In contrast, fSWT generates P_+ of up to 100 MPa in the treatment zone, although P_- is one order of magnitude lower. For a typical pressure waveform

generated by rSWT in water the frequency content is mainly below 100 kHz (Cleveland et al., 2007) meaning that wavelengths of approximately 15 mm or more should be dominant.

The rSWT treatment for plantar fasciitis typically consists of 3-6 sessions, each involving 1000-4000 impulses delivered at 10-20 pulses per second using a 15 mm diameter applicator (Furia and Rompe, 2007). Clinical studies indicate that SWT is successful in managing plantar fasciitis and other musculoskeletal disorders (Wang, 2012). Recent studies show that rSWT may be as effective as fSWT for this particular application (Chang et al., 2012). However, the mechanisms through which pressure waves act to enhance the healing process is still unknown (Wang, 2012). Current hypotheses include cavitation-induced micro-injury leading to neovascularisation (Chow and Cheing, 2007, Delius et al., 1995, Murata et al., 2007), biological response at the cellular level (Tamma et al., 2009), and pain management through the reduction of afferent sensory fibres (Ohtori et al., 2001). While being supported by experimental evidence, these existing theories do not provide a clear link between the mechanical stimulus and the induced favourable biological response. This is largely due to the fact that the pressure field that radial shock wave therapy generates in a non-homogeneous medium such as the human body is still not well explored; a recent modelling study on fSWT shows that the pressure field in the foot, including the focal region, differs significantly from that generated in experimental phantoms (Fagnan, 2010). In the research reported in this paper, finite element models of the radial shock wave device and foot were created to simulate the effect of rSWT for plantar fasciitis. The primary aim was to gain information on the pressure and energy fields generated by this therapeutic method in the anatomical structures of the foot. Also, the effect of the interfacing between the applicator and the foot was examined. Finally, the effect of more than one shock wave pulse was explored.

2 Methods

2.1 Finite element models

The finite element model of the shock wave device is shown in Figure 1a. The model was based on an actual shock wave hand piece with a standard 15 mm applicator. Only the front portion of the device was represented, as the process in which the projectile is accelerated was not simulated. The model comprised of the projectile, applicator, casing, and the two o-rings on which the applicator is suspended in the casing. The dimensions of the components were obtained from a shock wave device that was provided courtesy of the clinicians from the Royal Surrey County Hospital, Guildford, UK, with permission from the manufacturer. The applicator and the projectile were made of steel. The casing was represented as a rigid body. A compressible Mooney-Rivlin hyperelastic material model characterized by three constants (C_{01}, C_{10}, and D_1) was used for the o-rings (Table 1).

The foot geometry was reconstructed from MR images taken from a healthy volunteer (Figure 1b). The scans were obtained at 0.8 mm intervals in the sagittal plane using a Siemens Avanto MRI device, 1.5 T (Royal Surrey County Hospital, Guildford, UK). The segmentation was performed using the Simpleware software (Simpleware Ltd., Exeter, UK). The strategy for modelling was geared towards accurately capturing the transmission of pressure waves through the structures of the foot with emphasis on the region where the shock waves are applied. When representing the joints priority was placed on avoiding spurious discontinuities rather than on reproducing joint kinematics. The calcaneus, talus, tibia, and fibula were reconstructed as separate entities whereas the bones of the forefoot and hindfoot were fused into a single entity. The articulations were filled with 'cartilage tissue' representing all the tissues in a joint. The

cartilage fused the adjacent bones together, thus assuring the continuity of wave transmission. The central portion of the plantar fascia and the Achilles tendon were reconstructed as three-dimensional objects and were fully embedded in the surrounding soft tissue, which was modelled as a single entity. Material models for the foot components were selected from published finite element models of the foot (Lemmon et al., 1997, Jacob and Patil, 1999, Verdejo and Mills, 2002, Cheung et al., 2006, Goske et al., 2006, Tao et al. 2009, Shin et al., 2012). Preliminary numerical testing was carried out to assess a number of published material models for the plantar soft tissue and to test the effect of mesh size on the predicted pressure wave. The testing was performed by simulating the application of the shock wave device to a semi-infinite domain using different soft tissue material models and element sizes. To assess the material models the results for the generated pressure were compared with published data from in-vitro experiments (Cleveland et al., 2007, Ueberle and Rad, 2012). It was found that the material models which provide realistic acoustic properties of the soft tissue (i.e., longitudinal wave speed $c_L \approx 1500$ m/s) yielded results which were consistent with the experimentally obtained pressure waveforms reported in the literature. Informed by this finding the material model presented by Verdejo and Mills (2002) was selected for the soft tissue of the foot. The bone tissue was represented as a single homogeneous linear elastic material characterized by Young's modulus (E) and Poisson ratio (ν). The material constants were chosen so that the acoustic properties were in the experimentally reported range (Ogden et al., 2001). The Mooney-Rivlin hyperelastic material model was used for the soft tissue. The material constants C_{01} and C_{10} were chosen to exactly match the Ogden material model used by Verdejo and Mills (2002). The Mooney-Rivlin material model with C_{01}=0 (Neo-Hookean) was used for the plantar fascia, cartilage, and Achilles tendon. The constants were calculated from the linear elastic material parameters

reported in the literature as $C_{10}=G/2$, $D=2/K$, where G and K are the shear and bulk moduli, respectively. The material models and their parameters are summarised in Table 1. A density of 1000 kg m^{-3} is assumed if not otherwise stated.

All components of the device and foot models were meshed with constant stress four-noded tetrahedral elements with reduced integration. These elements are not prone to hourglassing, but they may exhibit volumetric locking for nearly incompressible materials. To avoid the latter the element formulation with additional node averaging of pressure (Halquist, 2003) was implemented for the o-rings and soft tissue. The meshing was performed using the ANSYS Workbench – Design Modeller (ANSYS Inc., Pittsburgh USA). A patch-independent meshing method was used in order to create a uniformly distributed mesh size suited for explicit dynamic simulations. The numerical testing carried out on a semi-infinite soft tissue domain suggested that the coarser mesh has a smoothing effect on the calculated pressure wave but it does not critically affect its key parameters, providing that the element size is 2 mm or smaller. Thus, for a 50 μs pressure waveform at 1 mm from the applicator tip, the values of P_+, P_-, and EFD obtained using 1.5 mm and 2 mm elements were within 10% of those obtained using 1 mm elements. On the other hand, the values of P_+, P_-, and EFD obtained using 2.5 mm and 3 mm elements were more than 30% lower than those obtained using the 1 mm elements. Consequently, the (maximum) element size of 2 mm was set for all foot components to assure accuracy at a reasonable computational cost. This is equivalent to fitting about 10 elements per typical wavelength, and it is consistent with the recommendation of theoretical studies (Bazant, 1978, Ham and Bathe, 2012). The device had to be meshed with smaller elements (0.5 mm for o-rings and 1 mm for the rest of the components) in order to preserve the shape accurately.

2.2 Simulation of shock wave therapy

The LS-DYNA finite element software (LS-DYNA Version 971, Livermore Software Technology Corp., Livermore, CA), was used to carry out the simulations. The shock wave device was positioned so that its axis of symmetry passed through the most affected segment of the plantar fascia near the insertion into the calcaneus (see Figure 1b). A tied contact was implemented between the components of the foot. For all components except the tibia, a non-reflecting boundary was implemented at the top surface, where the foot was 'cut' from the leg, in order to account for the waves being transmitted into the top portion of the leg. The top of the tibia, which stretched a further 90 mm upwards (Figure 1b), was fully constrained to provide static stability.

The dynamic simulation of the projectile-applicator collision was preceded by a static pre-load phase in which a force of 50 N was applied to the casing of the device in order to simulate the pre-load performed by clinicians. In the pre-load phase, the casing was restrained to move only in the axial direction and a sliding contact without friction was assigned between the applicator and the foot. For impact simulation the casing was fully constrained. In order to examine two extreme cases of device-foot interfacing the contact between the applicator and the foot was either set to tied, representing perfect interfacing, or it was kept as sliding, representing inadequate interfacing, e.g. due to a lack of coupling gel. The tied contact was chosen as the default. The initial condition was defined in terms of the projectile speed (V_0). Following experimental data provided by Benoit et al. (2009), three values of V_0 were considered: 9 m s^{-1}, 12.3 m s^{-1}, and 14.9 m s^{-1}. These values correspond to the device driving pressure settings of 1 bar, 2 bar, and 3 bar or more. The projectile speed of 12.3 m s^{-1} was chosen as the default. To simulate two shock wave pulses, two projectiles were used, and they were set to impact the

applicator 50 ms apart. The time step (Δt) was of the order of 10^{-8} s and was determined automatically based on the condition that for each element $\Delta t < d/c_L$, where d is the characteristic length of the element. The time step was adjusted dynamically during the simulation. Quasi-dynamic simulations with mass-weighted system damping were used for the pre-load phase by applying a global damping coefficient of 10^3 s^{-1} to all components of the model except the projectile. The damping was then set to zero for impact simulations. The computations were carried out on a work station (Dell Precision T7500, Two Intel Xeon X5667 processors, 88GB DDR3, 1333NHz). The simulation took approximately 12 hours for a single pulse and 36 hours for two pulses.

3 Results

The collision between the projectile and the applicator generated a stress wave in both objects. The projectile and applicator stayed in contact for approximately 10 μs during which time stress of the order of 10^2 MPa was generated. The duration of contact corresponds to the time needed for the stress wave to travel from the rear to the front end of the applicator and back. When the projectile and applicator separated, there were standing waves in both objects with an amplitude of the order of 10^1 MPa, and a characteristic timescale of the order of several μs. The parameters of the stress wave in the applicator are consistent with those observed by Benoit et al (2009) in a Hopkinson bar subjected to a rSWT source. In the applicator the wave was not plane. Rather, there were significant stress variations in the radial direction due to the complex shape. The maximal velocity at the front surface of the applicator was approximately $0.4V_0$ for all values of V_0 examined. The bulk movement of the applicator was mainly influenced by the interaction

between the o-rings acting as springs, and it occurred at much larger time scales than the stress wave. The period of this bulk motion was approximately 500 μs, while the maximal displacement of the applicator tip was roughly 0.2 mm. These values are consistent with the experimental data provided by the manufacturer (Wess, 2008).

When the device was applied to the foot, the stress waves were transmitted from the applicator to the plantar soft tissue in the form of radial pressure waves. However, due to very different acoustic impedances (ρc_L) the pressure amplitudes in the tissue was one order of magnitude lower than in the applicator. The highest pressure was generated at the interface between the applicator and the soft tissue. The maximum P_+ values were 5.25 MPa for V_0=9 m s^{-1}, 6.97 MPa for V_0=12.3 m s^{-1}, and 8.36 MPa for V_0=14.9 m s^{-1}. The maximum P_- values were -4.16 MPa for V_0=9 m s^{-1}, -5.77 MPa for V_0=12.3 m s^{-1}, and -7.14 MPa for V_0=14.9 m s^{-1}. The pressure waveforms recorded at the location of maximum P_- for the three different values of V_0 are shown in Figure 2a. It can be seen from the figure that the waveform shapes were independent of the projectile speeds, with the amplitudes being linearly related to V_0. Moreover, it was found that the peak positive pressure can be related to V_0 in a simple manner; thus, P_+ approximately equalled $0.4V_0\rho c_L$ which can be interpreted as maximal speed at the applicator tip multiplied by the acoustic impedance of the soft tissue. Figure 2b shows the pressure wave at the point where the axis of symmetry of the applicator crosses the plantar fascia. The pressure here was substantially lower than at the surface but the linear relation between V_0 and P_+ was preserved. Figures 2c and 2d show the comparison of the results for tied and sliding contacts between the applicator and the foot at the surface and at the plantar fascia, respectively. The positive peak in pressure waveforms were almost the same for the two types of contact

examined. However, the amplitude fell much more rapidly, and the negative pressure was far less pronounced for the sliding contact.

Figure 3 illustrates the general pattern of the pressure field generated in the foot. The section plane of the second ray displayed in the figure passes mid-way through the second metatarsal. The limits for the pressure contours are intentionally set at a low value of ± 0.1 MPa in order to easily identify zones of positive pressure (bright-shaded) and negative pressure (dark-shaded) in all foot components. The time (τ) is measured from the moment of projectile impact. At $\tau = 1.5\ \mu s$, the stress wave had been generated in the applicator and the projectile, but it still did not propagate into the soft tissue of the foot. Thus, the pressure in the foot was entirely due to pre-loading. At $\tau = 18.5\ \mu s$, the initial compression-rarefaction wave had been generated in the soft tissue and it traversed the plantar fascia reaching the calcaneus. The wavelength of this wave was approximately 20 mm. At $\tau = 28.5\ \mu s$, the first wave had progressed into the calcaneus and was followed by a train of compression-rarefaction waves. These waves emanated from the stress wave in the applicator and had a slightly shorter wavelength than the initial wave. It can be seen that the pressure waves changed direction when they progressed from the soft tissue into the bone, and that in the bone they propagated faster than in the soft tissue. This is even more obvious in the pressure distribution at $\tau = 38.5\ \mu s$, at which point the initial pressure wave passed through the superior surface of the calcaneus.

3.1 Pressure field and EFD

Figure 4 shows the distribution of P_+, P_-, and maximal von Mises stress recorded for $0 \le \tau \le 100\ \mu s$. The pre-load values of pressure/stress were subtracted so that the calculated fields apply to the effect of the shock wave alone. It can be seen from Figures 4a and 4b that for

P_+ and P_- the region of highest pressure stretches from the surface of the soft tissue to the boundary of the calcaneus including a short portion of the plantar fascia near the insertion. Beyond the limits of the calcaneus, the values of P_+ and P_- were negligible. In contrast, from Figure 4c it can be seen that the region of highest von Mises stress was in the calcaneus and in the portion of the plantar fascia near the insertion into the calcaneus. The highest value of von Mises stress was in the calcaneus and it equalled 3.7 MPa.

In order to obtain further quantitative information on the pressure field and EFD, their distribution was examined in more detail along the direction of the axis of symmetry of the applicator, up to 30 mm distance from the surface. The energy density was calculated from pressure waveforms (p(t)) as $\mathrm{EFD} = \frac{1}{\rho c_L} \int_0^{100\mu s} p^2 dt$. Figure 5a shows P_+ and P_- for three different values of V_0. It can be seen that P_+ and P_- decreased in proportion to the distance, with visible disruptions at the interfaces between the different tissues. Figure 5b compares P_+ and P_- for tied and sliding contacts between the applicator and the foot; in both cases V_0= 12.3 m s^{-1}. It can be seen from the figure that the type of contact had a strong effect on P_-, which was much lower for the sliding contact.

The distribution of EFD is shown in Figure 6. At the surface (zero distance), the values of EFD were 0.19 mJ mm^{-2} for V_0= 9 m s^{-1}, 0.36 mJ mm^{-2} for V_0= 12.3 m s^{-1}, and 0.53 mJ mm^{-2} for V_0= 14.9 m s^{-1}, as can be seen from Figure 6a. Therefore, the EFD level at the surface can be classified as medium-to-high. The values of EFD decreased with distance in an exponential way but they were significantly affected by the wave reflections at the interface of the different tissues. Thus, the EFD levelled-off between a depth of 6 and 10 mm. In the plantar fascia, the values of EFD were 0.027 mJ mm^{-2} for V_0= 9 m s^{-1}, 0.05 mJ mm^{-2} for V_0= 12.3 m s^{-1}, and 0.074

mJ mm^{-2} for V_0= 14.9 m s^{-1}. In the bone, the values of EFD were negligible. The type of contact had a very strong effect on EFD, which was markedly lower for the sliding contact as shown in Figure 6b.

3.2 Multiple Pulses

The effect of more than one shock wave pulse is illustrated in Figure 7 which shows pressure waveforms at the surface of the foot as well as the fluctuation of total energy (strain + kinetic) for the foot and plantar fascia. The pressure trace shown in Figure 7a indicates that the pressure was dissipated within 0.5 ms from the impact. The energy of the foot (Figure 7b), which equalled 40 mJ after the preload phase, jumped to 68 mJ after the first pulse. Given that the initial energy of the projectile equalled 256 mJ, this means that approximately 11% of its energy was delivered to the foot. The bulk of the energy was stored in the soft tissue (90%), followed by the plantar fascia and the calcaneus. The energy stored in the foot after the first pulse remained largely unchanged between the two successive pulses. The second shock wave pulse added an additional 28 mJ of energy, which indicates the possibility of the cumulative effect of multiple pulses. The same effect was observed for the plantar fascia which received about 1.1 mJ of energy (0.45% of the projectile energy) with each successive pulse (Figure 7c).

4 Discussion and Conclusions

The results for the pressure traces at, or just below, the front surface of the applicator were in good general agreement with in-vitro experimental results obtained by Cleveland et al. (2007), Benoit et al. (2009), and Ueberle and Rad (2012), in terms of amplitude and

characteristic time scale. It can be deduced from the simulations that the stress wave in the applicator resulting from the projectile impact has the crucial role in the generation of pressure waves in the tissue. The results further suggest that P_+ at the applicator interface can be accurately estimated as the product of the maximal speed at the applicator tip and the acoustic impedance of the tissue. For the applicator considered in this study, maximal velocity at the tip was in turn approximately 0.4 $V_{0,}$ but this relation will depend on the type of the applicator used. The pressure waveforms from a single pulse may persist for well over 50 μs . This may mean that the successive peaks of pressure observed experimentally by Ueberle and Rad (2012) in a silicone phantom may not be entirely due to wave reflections, as concluded by the authors, but may instead emanate from the persistent stress wave in the applicator. With this in mind, it may be useful to consider time intervals longer than the usual 20-25 μs when calculating EFD from pressure traces. The results also show that in the foot, EFD does not necessarily diminish in proportion to the square of the distance from the source, as it does in a homogeneous medium. In conclusion, it can be said that the values of EFD generated by rSWT between the surface of the foot and the calcaneus may be higher than what is estimated based on experiments in water baths and other phantoms.

When the pressure wave propagated into the interior of the foot, it was affected by the complex shape of the foot components and their different material properties. The pressure wave moved through the interface between the soft tissue and plantar fascia without much interference, but it was strongly affected by the interface between the bone and the soft tissue. The pressure amplitude fell considerably when the wave propagated into the bone, in spite of its acoustic impedance being higher than that of the soft tissue. The explanation may be that the incident longitudinal wave reaching the bone splits into transmitted longitudinal and shear waves, with

the transmitted shear wave carrying much of the energy. This conclusion is supported by the fact that the von Mises stresses generated by the pressure wave are the highest in the calcaneus. The same effect was reported by Cleveland and Sapozhnikov (2005) in the context of fSWT lithotripsy, and by Fagnan (2010) in the context of fSWT treatment of musculoskeletal disorders. This result also indicates that the plantar fasciitis shock wave treatment may have a secondary, in some cases possibly adverse, effect on the calcaneus.

Two contact types between the applicator and the soft tissue were examined: the tied contact, representing perfect interfacing, and the sliding contact representing the least effective interfacing. While the contact type did not have a significant effect on P_+, it strongly affected both P_- and EFD, which were both much lower in the case of the sliding contact. This result emphasizes the need for proper interfacing between the applicator and the tissue in clinical applications. It should be said that in reality, the coupling gel may not provide perfect acoustic coupling, meaning that perfect interfacing is not achievable in practice.

The results suggest that there may be a cumulative effect on the strain energy in the foot for multiple shock wave pulses. This is in spite of the fact that the pressure dissipated quickly, and it can be attributed to the shearing of the soft tissue which is propagated at a much lower speed (20 m s^{-1} or less) than the pressure waves. While the shear waves can still traverse the foot several times between two shock wave pulses, the bulk of them are reflected back and do not reach the non-reflective boundary at the top of the foot. Consequently, the energy inside the foot remains almost constant. It should be said that with large number of successive pulses, non-linear effects may eventually lead to saturation. Also, tissue viscoelasticity, which was not considered in this study, may in reality act to diminish or completely dismiss the energy

accumulation. Nevertheless, the energy accumulation effect deserves further attention in future studies, which should consider large number of pulses and viscoelasticity of the soft tissues.

The model predicts that the magnitude of negative pressure at the plantar fascia and the surrounding soft tissue can be beyond 1.5 MPa, which is the lowest threshold for the onset of cavitation in the tissue as suggested by Coleman et al. (1995). Therefore, cavitation could potentially play a role in enhancing the healing process. If cavitation indeed is an important healing mechanism, this may explain why some clinical studies conclude rSWT is equally effective in treating plantar fasciitis as fSWT (Chang et al., 2012), as negative pressures generated by the two methods are of the same order of magnitude. A more rigorous analysis of the feasibility of this physical mechanism is required before any firm conclusions are made.

The objective of this study was to gain a general picture of the pressure field generated in the entire foot by the rSWT treatment. In order to construct a finite element model of the whole foot that can be run at a reasonable computational cost, the soft tissue was represented as a single entity and meshed so that only the dominant wavelengths were captured. While the preliminary numerical testing conducted on a simple geometry suggested that the mesh used in this model should be sufficiently fine to accurately capture key pressure wave parameters, this conclusion will not necessarily translate to a geometrically complex non-homogeneous object such as the human foot. As one of the conclusions from this study is that the effective region of the rSWT treatment is in the immediate vicinity of the source, it can be said that the future models could focus on a small segment of the foot which could then be presented in a more detailed way in terms of the geometry, material properties of different soft and connective tissues, and the mesh size. In addition, the effect of more elaborate material models on the results should be pursued in the future modelling studies, including the effect of viscosity (for the soft tissues), poroelasticity,

and inhomogeneity (for the bone). Finally, it should be stressed that experimental validation is needed before any definite conclusions are drawn from the results of this study.

Acknowledgments

This project has been conducted as part of the first author's PhD which was generously funded by the Saudi Food and Drug Authority (SFDA)

References

Bazant, Z. P. 1978. Spurious Reflection of Elastic-Waves in Nonuniform Finite-Element Grids. Computer Methods in Applied Mechanics and Engineering, 16: 91-100.

Benoit, M., Giovanola, J., Curnier, A., Agbeviade, K., Donnet, M. 2009. Characterization of pressure wave propagation in biological tissues. In: DYMAT 2009 - 9th International Conference on the Mechanical and Physical Behaviour of Materials under Dynamic Loading, Vol. 1. Brussels, Belgium; September 7-11, 2009.

Chang, K. V., Chen, S. Y., Chen, W. S., Tu, Y. K., Chien, K. L. 2012. Comparative effectiveness of focused shock wave therapy of different intensity levels and radial shock wave therapy for treating plantar fasciitis: a systematic review and network meta-analysis. Arch Phys Med Rehabil, 93**:** 1259-68.

Cheung, J. T., An, K. N. & Zhang, M. 2006. Consequences of partial and total plantar fascia release: a finite element study. Foot Ankle Int, 27**:** 125-32.

Chow, I. H., Cheing, G. L. 2007. Comparison of different energy densities of extracorporeal shock wave therapy (ESWT) for the management of chronic heel pain. Clin Rehabil, 21**:** 131-41.

Cleveland, R. O., Chitnis, P. V., McClure, S. R. 2007. Acoustic field of a ballistic shock wave therapy device. Ultrasound Med Biol, 33**:** 1327-35.

Cleveland, R. O., Sapozhnikov, O. A. 2005. Modeling elastic wave propagation in kidney stones with application to shock wave lithotripsy. J Acoust Soc Am, 118**:** 2667-76.

Coleman, A. J., Kodama, T., Choi, M. J., Adams, T., Saunders, J. E. 1995. The cavitation threshold of human tissue exposed to 0.2-MHz pulsed ultrasound: preliminary measurements based on a study of clinical lithotripsy. Ultrasound Med Biol, 21**:** 405-17.

Crawford, F., Atkins, D., Edwards, J. 2002. interventions for treating plantar heel pain. The Foot, 11**:** 228 - 250.

Delius, M., Draenert, K., Al Diek, Y., Draenert, Y. 1995. Biological effects of shock waves: in vivo effect of high energy pulses on rabbit bone. *Ultrasound Med Biol,* 21**:** 1219-25.

Fagnan, K. 2010. High resolution finite volume methods for extracorporeal shock wave therapy. [Ph.D. Thesis]. Seattle (WA): University of Washington.

Furia, J., Rompe, J. 2007. Extracorporeal shock wave therapy in the treatment of chronic plantar fasciitis and Achilles tendinopathy. Curr Opin Orthop, 18**:** 102-11.

Goske, S., Erdemir, A., Petre, M., Budhabhatti, S., Cavanagh, P. R. 2006. Reduction of plantar heel pressures: Insole design using finite element analysis. J Biomech, 39**:** 2363-70.

Halquist 2003. LS-DYNA Keyword User's Manual: Version 970, Livermore Software Technology Corporation. Livermore (CA).

Ham, S., Bathe, K. J. 2012. A finite element method enriched for wave propagation problems. Computers & Structures, 94-95: 1-12.

Jacob, S., Patil, M. K. 1999. Three-dimensional foot modeling and analysis of stresses in normal and early stage Hansen's disease with muscle paralysis. J Rehabil Res Dev, 36**:** 252-63.

League, A. C. 2008. Current concepts review: plantar fasciitis. Foot Ankle Int, 29**:** 358-66.

Lemmon, D., Shiang, T. Y., Hashmi, A., Ulbrecht, J., Cavanagh, P. 1997. The effect of insole in therapeutic footwear- A finite element approach. Journal of Biomechanics, 30**:** 615-620.

Liao, C., Huang, W., Wang, Y., Suo, S. & Liu, Y. 2013. Fluid-solid interaction model for hydraulic reciprocating O-ring seals. Chinese Journal of Mechanical Engineering, 26**:** 85-94.

McClure, S. , Dorfmuller, C. 2003. Extracorporeal shock wave therapy: theory and equipment. Clin Tech Equine Pract, 2**:** 348-57.

Murata, R., Nakagawa, K., Ohtori, S., Ochiai, N., Arai, M., Saisu, T., Sasho, T., Takahashi, K., Moriya, H. 2007. The effects of radial shock waves on gene transfer in rabbit chondrocytes in vitro. Osteoarthritis Cartilage, 15**:** 1275-82.

Ogden, J. A., Toth-Kischkat, A., Schultheiss, R. 2001. Principles of shock wave therapy. Clin Orthop Relat Res**, 387 :** 8-17.

Ohtori, S., Inoue, G., Mannoji, C., Saisu, T., Takahashi, K., Mitsuhashi, S., Wada, Y., Takahashi, K., Yamagata, M., Moriya, H. 2001. Shock wave application to rat skin induces degeneration and reinnervation of sensory nerve fibres. Neurosci Lett, 315**:** 57-60.

Rome, K., Saxelby, J. 2005. Critical review: assessment and management of plantar fasciitis. British Journal of Podiatry, 8**:**2 - 15

Rompe, J. D., Furia, J., Weil, L. & Maffulli, N. 2007. Shock wave therapy for chronic plantar fasciopathy. *Br* Med Bull, 81-82**:** 183-208.

Shin, J., Yue, N., Untaroiu, C. D. 2012. A finite element model of the foot and ankle for automotive impact applications. Ann Biomed Eng, 40**:** 2519-31.

Tamma, R., Dell'Endice, S., Notarnicola, A., Moretti, L., Patella, S., Patella, V., Zallone, A. & Moretti, B. 2009. Extracorporeal shock waves stimulate osteoblast activities. Ultrasound Med Biol, 35**:** 2093-100.

Tao, K., Wang, D., Wang, X., Liu, A., Nester, C., Howard, D. 2009. An in vivo experimental validation of a computational model of human foot. J Bionic Eng, 6**:** 387 - 97.

Ueberle, F., Rad, A. J. 2012. Ballistic Pain Therapy Devices: Measurement of Pressure Pulse Parameters. *Biomed Tech.* 57 (Suppl. 1) :700 - 7003.

Verdejo, R., Mills, N. J. 2002. Performance of EVA foam in running shoes. The Engineering of Sport, 4**:** 580-87.

Wang, C. J. 2012. Extracorporeal shockwave therapy in musculoskeletal disorders. J Orthop Surg Res, 7**:** 11.

Wess, O. 2008. Physics and technology of shock wave and pressure wave therapy [Internet]. c2008-2015. Tägerwilen: Storz Medical. [cited 2015 Jul 14]. Available from : http://eswt.net/pdfs/Physics-of-SWT-and-PWT.pdf

Table 1: Material properties of model components

Component	Material Model	Constants	Source
Projectile and Applicator	Linear elastic	$E=2.0\times10^{11}$ Pa; $\nu=0.3$; $\rho=7800$ kg m^{-3}	
Casing	Rigid	$\rho=7800$ kg m^{-3}	
O-rings	Mooney-Rivlin	$C_{01}=0.483\times10^{6}$ Pa; $C_{10}=1.933\times10^{6}$ Pa; $D_1=1.0\times10^{-9}$ Pa^{-1}; $\rho=1150$ kg m^{-3}	Liao et al. (2013)
Bone	Linear elastic	$E=7.3\times10^{9}$ Pa; $\nu=0.3$; $\rho=1600$ kg m^{-3}	Jacob and Patil (1999)
Cartilage	Neo-Hookean	$C_{10}=1.67\times10^{7}$ Pa; $D_1=1.2\times10^{-9}$ Pa^{-1}	(Jacob and Patil, 1999);
Plantar fascia	Neo-Hookean	$C_{10}=6.0\times10^{7}$ Pa; $D_1=1.028\times10^{-9}$ Pa^{-1}	Tao et al. (2009)
Achilles tendon	Neo-Hookean	$C_{10}=2.1\times10^{8}$ Pa; $D_1=1.0\times10^{-9}$ Pa^{-1}	Tao et al. (2009)
Soft tissue	Mooney-Rivlin	$C_{01}=C_{10}=1.0\times10^{5}$ Pa; $D_1=1.0\times10^{-9}$ Pa^{-1}	Verdejo and Mills (2002)

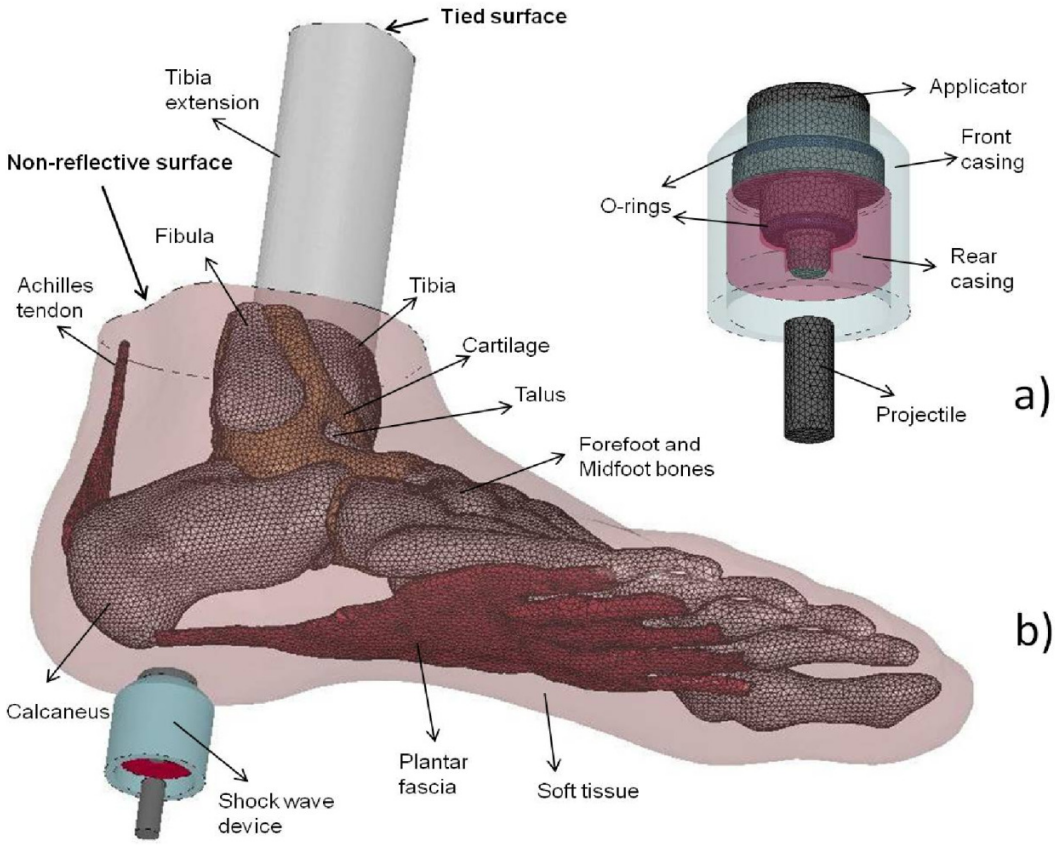

Fig. 1: Finite element models of: a) the shock wave device; b) the foot.

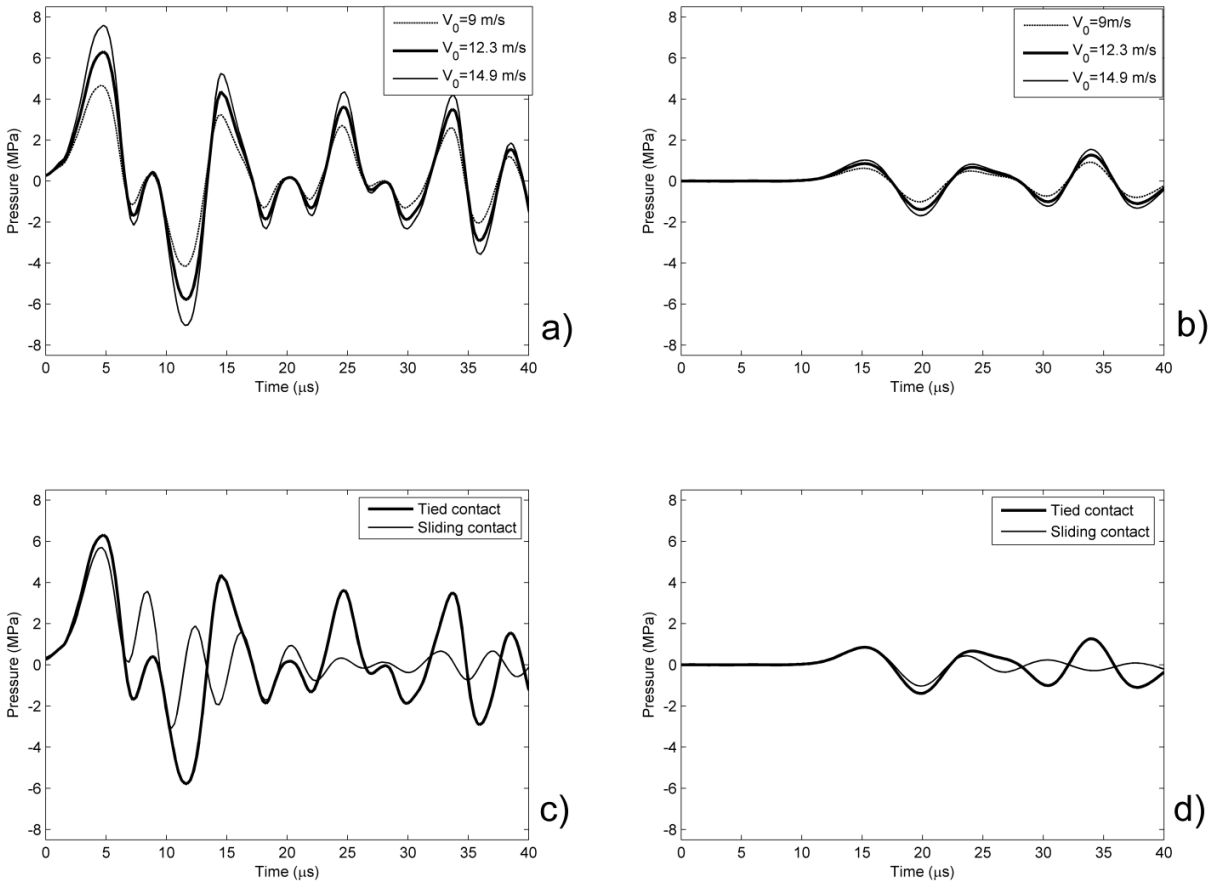

Fig. 2: Pressure traces for three different values of V_0. a) at the interface between the applicator and the foot, b) at affected region of the plantar fascia. Pressure traces for tied and sliding contacts between the applicator and tissue with V_0=12.3 m s^{-1}. c) at the interface between the applicator and the foot, d) at affected region of the plantar fascia.

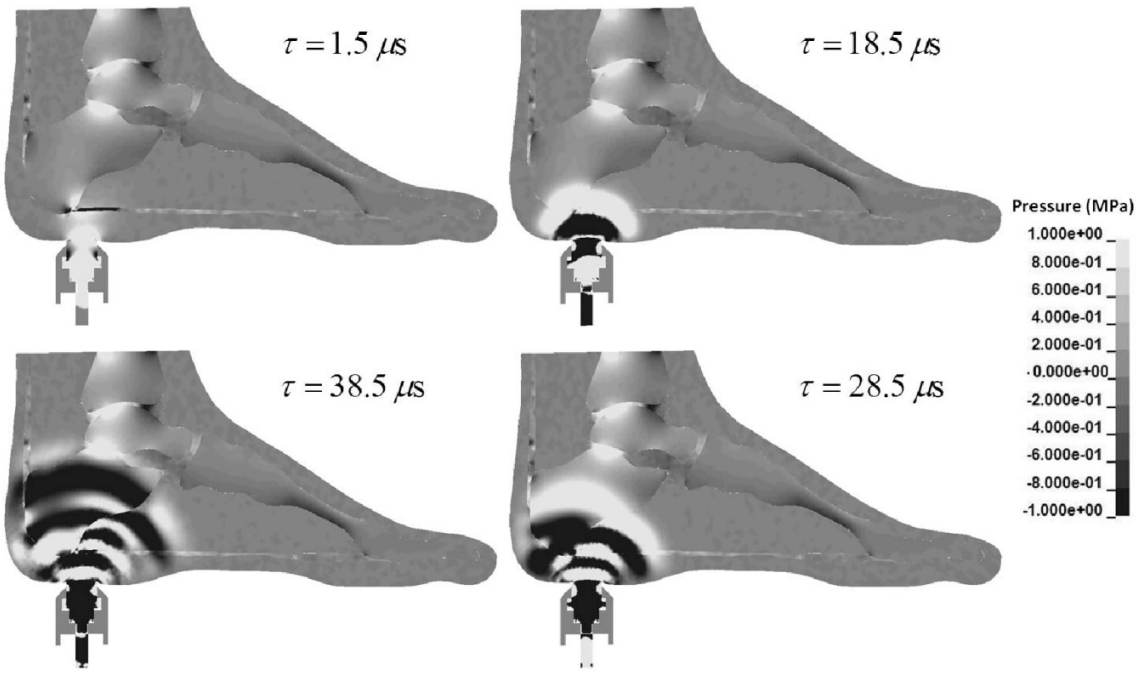

Fig. 3: Pressure field in the plane of the second ray of the foot for different points in time.

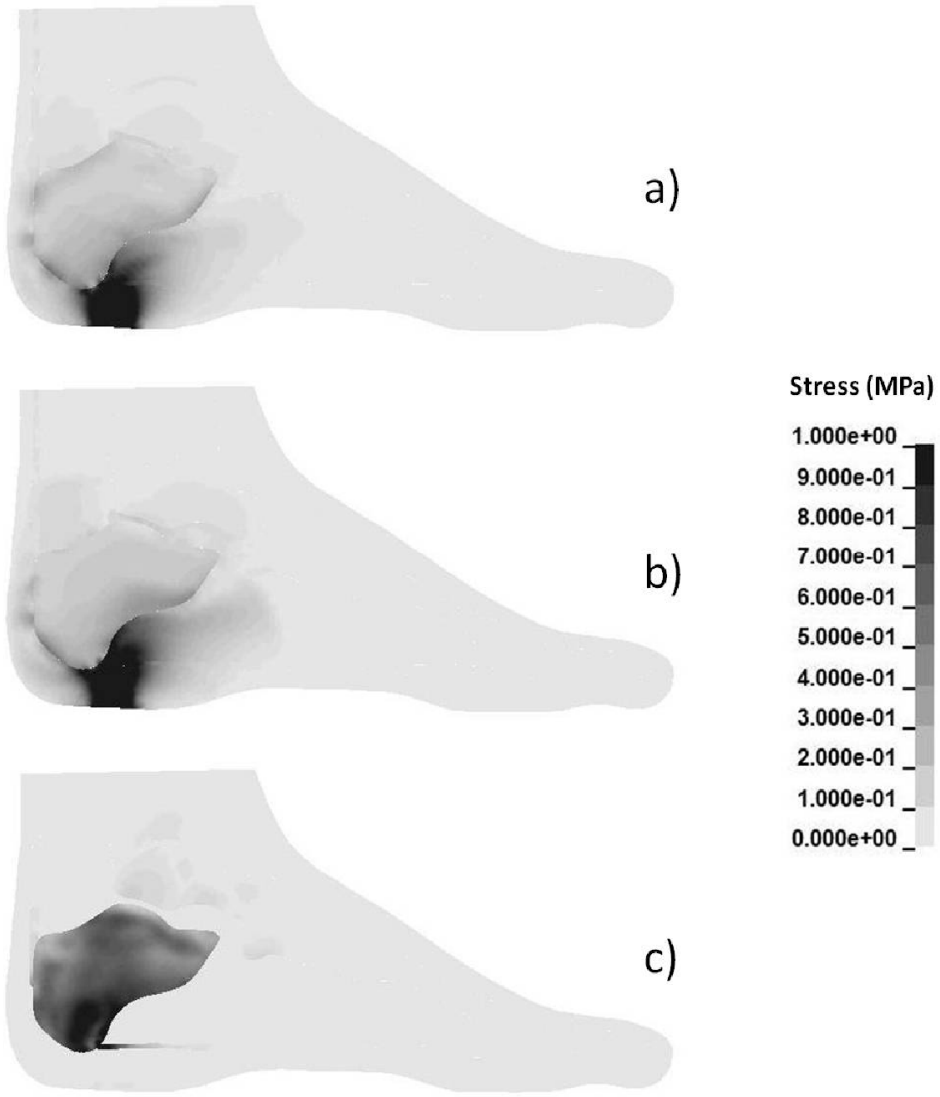

Fig. 4: The distribution of P_+, P-, and peak von Mises stress. The results are obtained for V_0=12.3 m s^{-1}.

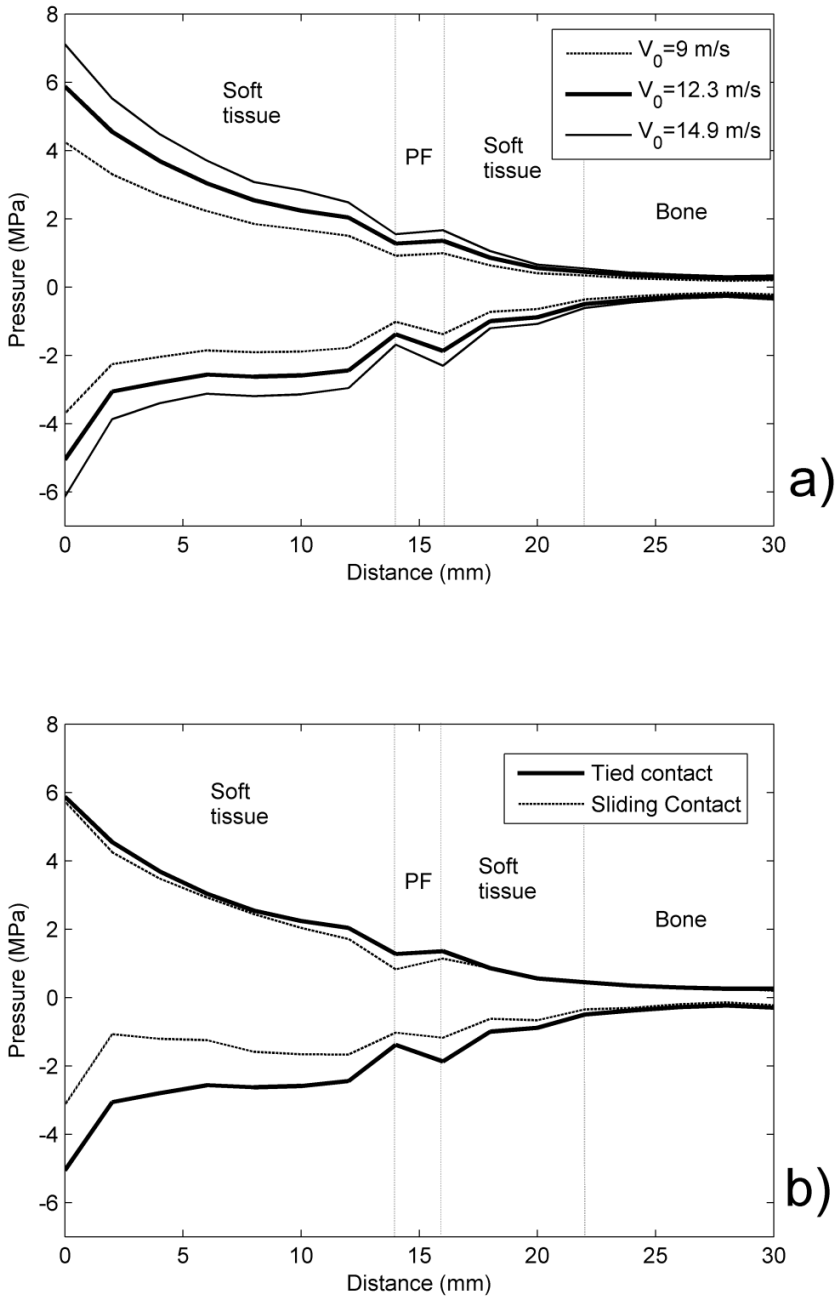

Fig. 5: The distribution of P_+ and P_- in the foot, along the direction of the axis of symmetry of the applicator: a) for three different values of V_0; b) for tied and sliding contacts between the applicator and tissue with V_0=12.3 m s^{-1}. The distance is measured from the surface of the foot.

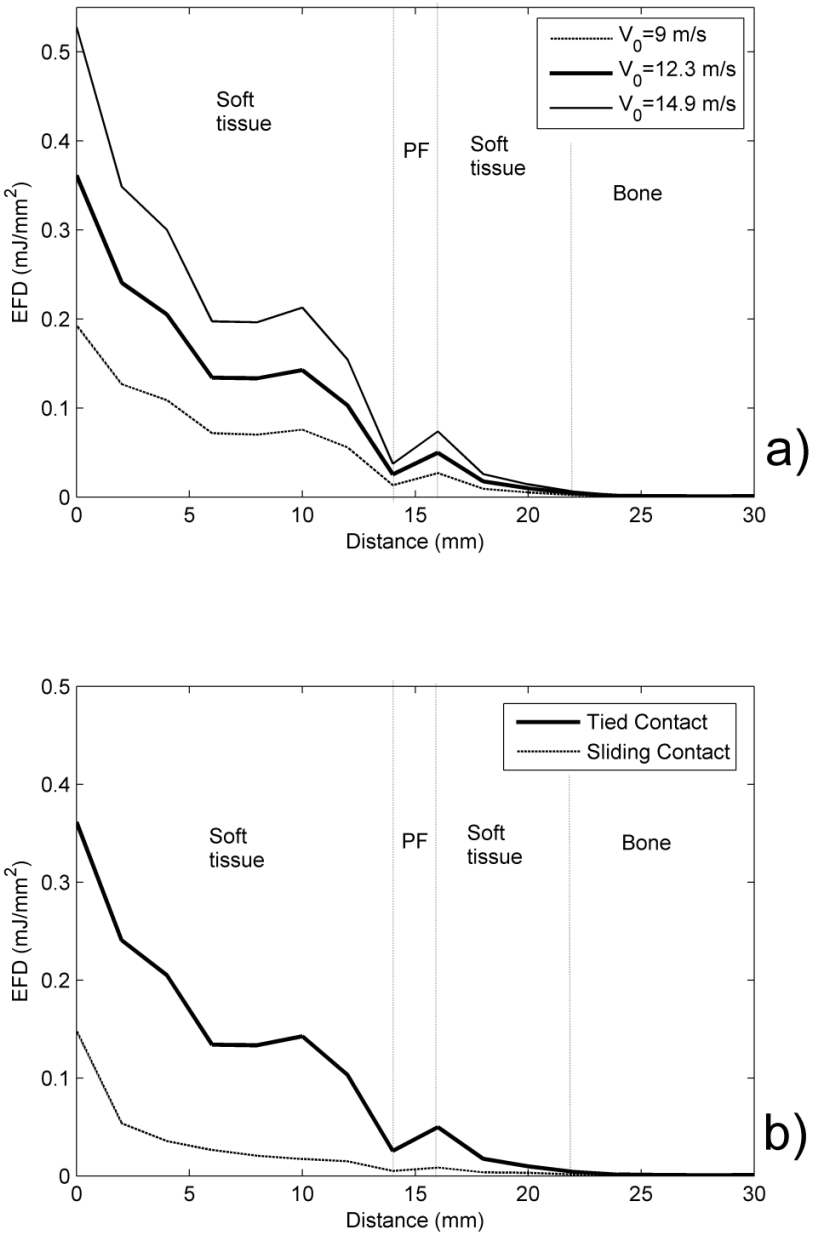

Fig. 6: The distribution of EFD in the foot along the direction of the axis of symmetry of the applicator: a) for three different values of V_0; b) for tied and sliding contacts between the applicator and tissue with V_0=12.3 m s^{-1} .

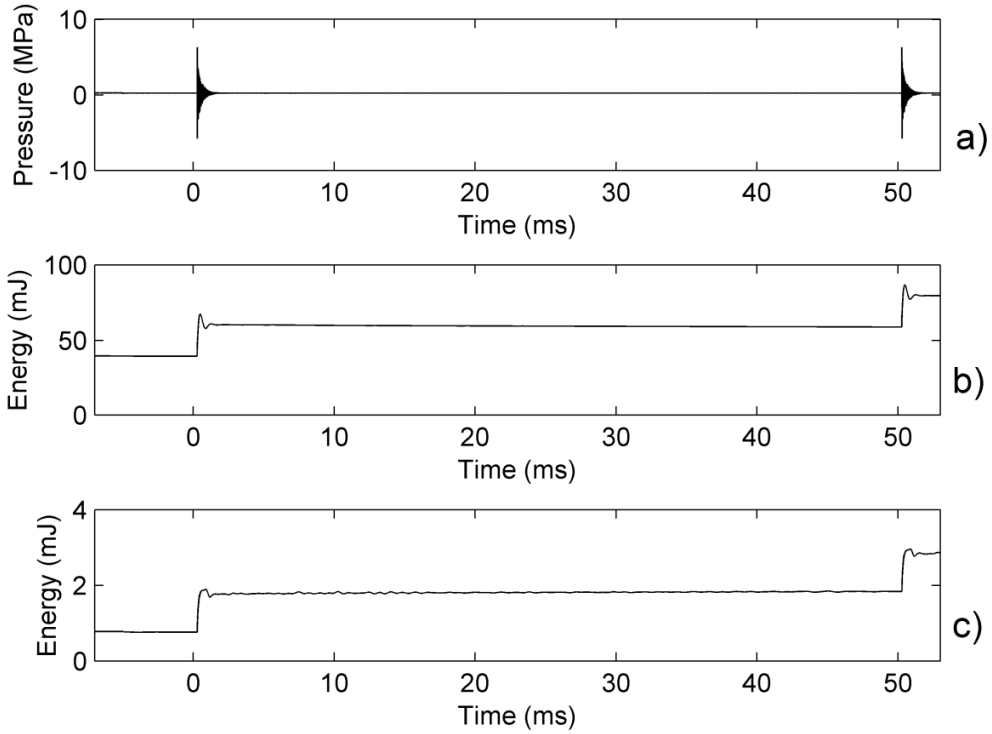

Fig. 7: Two successive shock wave pulses: a) pressure at the interface between the applicator and the foot; b) total energy stored in the foot; c) total energy stored in the plantar fascia.